(A New Proposal to Jefferson Lab PAC27)
Neutron Tagged bound proton structure to probe the Origin of the EMC Effect

J.P. Chen, P. Degtiarenko, E. Chudakov, J. Gomez, D. Higinbotham, B. Reitz,
B. Wojtsekhowski (Spokesperson)
Jefferson Lab, Newport News, VA 23606

N. Liyanage (Spokesperson and contact person), V. Nelyubin,
B. Norum, K. Wang, B. Craver, R. Chang
University of Virginia, Charlottesville, VA 22904

J.R.M. Annand
University of Glasgow, Glasgow G128QQ, Scotland, UK

B. Sawatzki
Temple University, Philadelphia, PA 19122

November 30, 2004

Abstract

Deep Inelastic Scattering of high energy electrons off the proton bound in the deuteron in coincidence with a slow backward going neutron will be investigated in Hall A using a large acceptance BigBite spectrometer. We will study a variation of the ratio of the bound proton cross section to the free proton cross section over a grid of Bjorken scaling variable x and the recoil neutron momentum. This information allow to discriminate between different hypotheses on the origin of the nuclear EMC effect.

1 Introduction

It has been more than two decades since the discovery of the EMC effect. However, its origin still remains a mystery. There are many theoretical models that attempt to explain the EMC effect. They range from models that explain the EMC effect entirely in terms of hadronic degrees of freedom of nuclear force to those attribute the effect to the deformation of the nucleonic wave function. Since the publication of the EMC data in 1983 [1], there have been many precision inclusive measurements of EMC effect on various nuclear targets over a large range of x and Q^2 [2, 3, 4, 5]. This large collection of data has revealed several important facts about the EMC effect:

- the x dependent shape of the EMC effect is roughly independent of the target atomic mass number, A,
- the increase in the EMC effect at a given x with increasing A can be described well as a function of A or as a linear function of nuclear density,
- the EMC effect does not depend on Q^2.

For a review of the published EMC effect data and theoretical models, see [6]. Hall C Experiment E03-013 [7] is currently collecting inclusive data for a precision measurement of the EMC effect on ^3He and ^4He.

The models based on very different physics ideas can more or less fit the x and the A dependence of the EMC effect. Therefore is has not been possible to distinguish between the models to identify possible cause or causes of the EMC effect. What has been missing in the available data-sets is a measurement of the variation of the effect as the binding of the nucleon increases and it becomes more and more off-shell. In the case of deuteron, the recoil momentum of the spectator nucleon is a measure of the nuclear binding strength. A comparison of several available EMC effect models by Melnitchouk *et al.* [8] has indicated that the models based on different physics ideas make vastly different predictions for the EMC effect as a function of the nuclear binding strength (or the recoil momentum of the spectator in case of the deuteron). Therefore, a precision measurement of the EMC effect for the bound proton in a deuteron target as a function of the recoil neutron momentum can be used to distinguish between different classes of models. This may help us understand the origins of the EMC effect.

At Jefferson lab Hall A we can measure the ratio of cross section for a bound proton in deuteron to that of a free proton as a function of the recoil neutron momentum at different values of x, up to $x \approx 0.6$, in the DIS region ($1 < Q^2 < 5$ (GeV/c)^2 and $W^2 > 4$ GeV^2). The accessible range of the recoil neutron momentum would be from as low as 50 MeV/c, where the proton is expected to be barely bound, to about 400 MeV/c, where the proton is significantly off-shell. We will select extreme backward kinematics and low transverse momentum for the recoil neutron detection. The neutron is in spectator kinematics in this case. Furthermore, Final State Interaction (FSI) effects have been predicted to be minimal for these kinematics [8]. Since it is the point-to-point variation of the EMC effect for the bound proton that is interesting, we will form the ratio of the bound proton cross-section at different values of x to the bound proton cross-section measured at $x = 0.2$, where EMC effect is minimal. Forming this cross section ratio would divide out experimental systematics such as the neutron detection efficiency as well as theoretical uncertainties such as the dependence on the deuteron wave function. In this proposal we will demonstrate that we can measure the relevant cross section ratio to 1% level over a fine grid of x and the recoil neutron momentum.

Jefferson lab Hall B experiment E-94-102 [9] recently measured the cross section for the bound neutron in the deuteron by tagging the proton over the recoil momentum range of 250 MeV/c to 400 MeV/c. However in this case there is no free neutron cross section to compare the bound cross section to and hence one has to rely on models to estimate the degree of the EMC effect as a function of the recoil momentum. In contrast, in the proposed experiment the ratio of the bound cross section to the free cross section, measured back-to-back, allows us to estimate the level of the EMC effect in a model independent way. Furthermore in the proposed experiment we will detect the spectator neutrons down to a recoil momentum of 50 MeV/c, which corresponds to barely 1 MeV in kinetic energy. This would allow us to study the evolution of the EMC effect from a barely bound to a strongly bound proton.

While it is vitally important to understand the origin of the EMC effect on its own right, it is also important for the extraction of the neutron structure functions from nuclear targets. An unambiguous measurement of the F_2^n/F_2^p ratio is of fundamental importance as has been pointed out at Jefferson lab many times over the last few years. It is the EMC effect in deuteron that prevents an unambiguous extraction of F_2^n at large values of x [10]. Hall B Bonus experiment [11] plans to measure the proton tagged F_2^n at low recoil momenta ($P > 70$ MeV/c) to minimize nuclear effects. While the nuclear effects are expected to be generally small in the momentum range of the Bonus experiment ($P \approx 100$ MeV/c), different models of the EMC effect predict different levels of effect, ranging from less than 1% to about 3-4% level for $x \approx 0.6$. Once again, since there is no free nucleon measurement to compare to one has to rely on theoretical models to correct for this effect. On the other hand using the proposed experiment we can accurately measure the level of the EMC effect for the proton over the recoil momentum range of the Bonus experiment, and then one can use these data to constrain the models to perform more effective corrections to the F_2^n data. The influence of the EMC effect on the F_2^n results has been shown to increase rapidly with increasing x. Since measuring the F_2^n/F_2^p at $x \to 1$ is one of the major experimental initiatives for the CEBAF 12 GeV upgrade, understanding the evolution of the EMC effect as a function of the spectator momentum would be of great importance to the 12 GeV program.

2 The Formalism

2.1 Inclusive Deep Inelastic Scattering

The inclusive cross section in the DIS region can be written in terms of the structure functions F_1 and F_2 as

$$\frac{\mathrm{d}^2\sigma}{\mathrm{d}\Omega \mathrm{d}E'} = \left(\frac{\mathrm{d}\sigma}{\mathrm{d}\Omega}\right)_{Mott} \left[\frac{1}{\nu} F_2(x, Q^2) + \frac{2}{M} F_1(x, Q^2) \tan^2 \frac{\theta}{2}\right] , \tag{1}$$

where θ is the scattering angle of the electron in the laboratory frame. The four momentum transfer, $Q^2 = -q^2$, is given by

$$Q^2 = 4EE' \sin^2 \frac{\theta}{2} , \tag{2}$$

scaling variable x,

$$x = \frac{Q^2}{2p \cdot q} , \tag{3}$$

(p is the initial four momentum of the struck nucleon) and the Mott cross section,

$$\left(\frac{\mathrm{d}\sigma}{\mathrm{d}\Omega}\right)_{Mott} = \frac{\alpha^2 \cos^2 \frac{\theta}{2}}{4E^2 \sin^4 \frac{\theta}{2}} = \frac{\alpha^2 \cos^2 \frac{\theta}{2}}{Q^4} \frac{E'}{E} \tag{4}$$

where α is the fine structure constant. $F_1(x, Q^2)$ and $F_2(x, Q^2)$ are related to each other through R, the ratio between longitudinal and transverse virtual photon cross sections,

$$F_1(x, Q^2) = \frac{F_2(x, Q^2)(1 + \gamma^2)}{2x\Big(1 + R(x, Q^2)\Big)} \tag{5}$$

where $\gamma^2 = (2Mx)^2/Q^2$.

Thus in the case of inclusive scattering off a free proton, the structure function $F_2(x, Q^2)$ can be extracted from the cross section:

$$F_2^{free}(x, Q^2) = \left[\frac{d^2\sigma/d\Omega dE'}{(d\sigma/d\Omega)_{Mott}}\right] \left[\frac{\nu\epsilon(1 + R(x, Q^2))}{1 + \epsilon R(x, Q^2)}\right] \tag{6}$$

2.2 Spectator tagging measurement

A convenient choice of independent variables for a spectator tagging measurement includes Q^2 and x, as well as the transverse momentum p_t^s and the light cone momentum fraction α^s of the spectator nucleon.

$$\alpha^s = \frac{E^s - p_z^s}{M}$$

where p_z^s is the spectator momentum along the q vector. The detection of the recoil nucleon in extreme backward angles such that $p_t \approx 0$ ensures that FSI effects are minimal and the recoil nucleon was in spectator kinematics. For this kinematic arrangement $\alpha^s \geq 1$.

When the struck nucleon is initially at rest $p \cdot q = M\nu$ (where ν is the energy transfer in the lab frame) and x is given by

$$x = \frac{Q^2}{2p \cdot q} = \frac{Q^2}{2M\nu} = x_{Bj} \ , \tag{7}$$

and

$$W^2 = M^2 - Q^2 + 2p \cdot q = M^2 - Q^2 + 2M\nu \ , \tag{8}$$

However, when the electron scatters off a bound nucleon moving with a momentum $\vec{p}$, where $\vec{p} = \vec{p}^{sp}$ in the spectator picture, x and W^2 are different from x and W^2 calculated in equations 7 and **??** assuming a nucleon stationary in the lab frame. Thus in this proposal we use the notation

$$x' = \frac{Q^2}{2p \cdot q} \ , \tag{9}$$

and

$$W^{2\prime} = M^2 - Q^2 + 2p \cdot q \ , \tag{10}$$

and explicitly calculate x' and W'^2 for each α^s bin using the spectator picture: $\vec{p} = \vec{p}^{sp}$. Note that in the limit $q/\nu \to 1$ x' is related to x_{Bj} by

$$x' \approx \frac{x}{2 - \alpha^s} \ , \tag{11}$$

In the nuclear impulse approximation, where incoherent inelastic scattering takes place from individual nucleons in the nucleus, the semi-inclusive cross section for the reaction D(e,e′N)X can be written as a product of the deuteron spectral function $S(\alpha^s, p_t)$ and the effective structure function $F_{2,p}^{eff}$ [8]

$$\frac{d\sigma^{eD \to enX}}{dx dW^2 d(\log \alpha^s) d^2 p_t} \approx \frac{2\alpha_{em}^2}{Q^4}(1-y) S(\alpha^s, p_t) F_{2,p}^{eff}\left(\frac{x}{2-\alpha^s}, p_t, Q^2\right) \tag{12}$$

From equations 6 and 12 we see that one can access the ratio $F_{2,p}^{eff}/F_{2,p}^{free}$ through,

$$\frac{F_{2,p}^{eff}}{F_{2,p}^{free}} \propto \frac{\sigma(D(e,e',N)X)_{(x,\alpha^s,p_t,Q^2)}}{\sigma(p(e,e')X)_{(x',Q^2)}} \tag{13}$$

where $x' = x/(2 - \alpha^s)$.

However there are practical difficulties in accessing $F_{2,p}^{eff}$ or ($F_{2,n}^{eff}$) from $\sigma^{eD \to enX}$ (or from $\sigma^{eD \to epX}$). The uncertainties in spectator nucleon detection efficiency and solid angle will dominate this cross section measurement. Even if such an absolute semi-inclusive cross section is measured, the uncertainty in the deuteron spectral function would dominate the uncertainly in the extracted $F_{2,p}^{eff}$, especially at high recoil momenta. These uncertainties are only dependent on the spectator neutron momentum and are not correlated with x or Q^2 for the electron scattering off the proton. Thus, all these uncertainties can be divided out by forming the ratio between $\sigma^{eD\to enX}$ at a given x and $\sigma^{eD\to enX}$ at $x = 0.2$, where the observed EMC effect in inclusive scattering is small [22, 30]:

$$G(\alpha^s, p_t, x_1, x_2, Q^2) \equiv \frac{d\sigma(x_1, \alpha^s, p_t, Q^2)}{dxdW^2 d(\log\alpha^s)d^2\mathbf{p}_t} \Big/ \frac{d\sigma(x_2, \alpha^s, p_t, Q^2)}{dxdW^2 d(\log\alpha^s)d^2\mathbf{p}_t}$$
$$= \frac{F_{2,p}^{eff}(x_1/(2-\alpha^s), p_t, Q^2)}{F_{2,p}^{eff}(x_2/(2-\alpha^s), p_t, Q^2)}. \qquad (14)$$

where $x_2/(2-\alpha_s) = 0.2$.

Furthermore, to the level the FSI are independent of x, this ratio will divide out the FSI as well.

In [8] Melnitchouk *et al.* compared the predictions from three different classes of EMC effects models for the ratios $F_{2,p}^{eff}/F_{2,p}^{free}$ and $G(\alpha^s, p_t, x_1, x_2, Q^2)$ as a function of α^s. The models they considered were:

- **Binding Models**: There are many theoretical models [22, 33, 34, 35, 36, 37, 38, 39, 40] that try to explain the main features of the EMC effect in terms of conventional nuclear degrees of freedom, nucleons and pions, responsible for the binding in nuclei. In many of these models the structure functions of the bound nucleon only plays a minor role.

- **Color Screening Model of Suppression of Point-Like Configurations (PLC) in Bound Nucleons** The increase in the EMC effect with x may indicate that the high momentum components of the quark distribution in the nucleon might play an important role in the EMC effect. For these high momentum configurations the three quarks are likely to be close together. In the Color Screening Model of Frankfurt and Strikman [22, 30] they assume that for large x the dominant contribution to $F_{2,N}(x, Q^2)$ is given by the Point-Like Configurations (PLC) of partons which weakly interact with the other nucleons. They argue that the suppression of this component in a bound nucleon is the main source of the EMC effect.

- **Rescaling model, QCD Radiation - Quark Delocalization**: Some authors have argued[44, 46, 47, 48] that due to the quark delocalization (or enlargement -swelling- of the confinement radius) of a bound nucleon, it radiates gluon more efficiently than a free nucleon. In this model the strength is shifted in x due to this extra gluon radiation when the electron scatters off a bound nucleon.

Figures 1 and 2 show the comparison between these predictions at $x = 0.6$. As figure 2 indicates, a measurement of $G(\alpha_s, p_T, x_1, x_2, Q^2)$ vs. α^s would help distinguish between models.

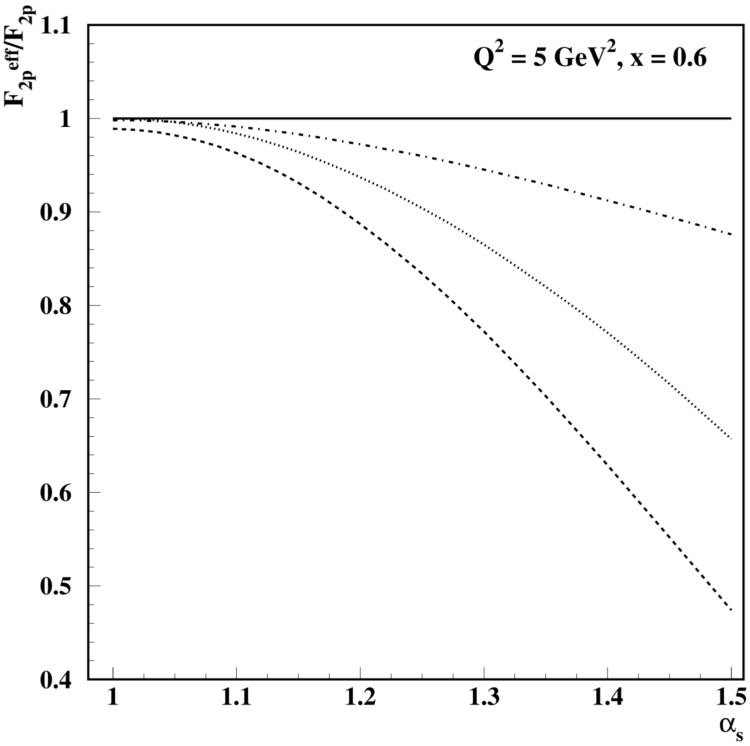

Figure 1: The α^s dependence of $F_{2,p}^{eff}/F_{2,p}^{free}$ ratio at $x = 0.6$ from [8]. The dashed line is the PLC suppression model, dotted is the rescaling model and dot-dashed the Binding model

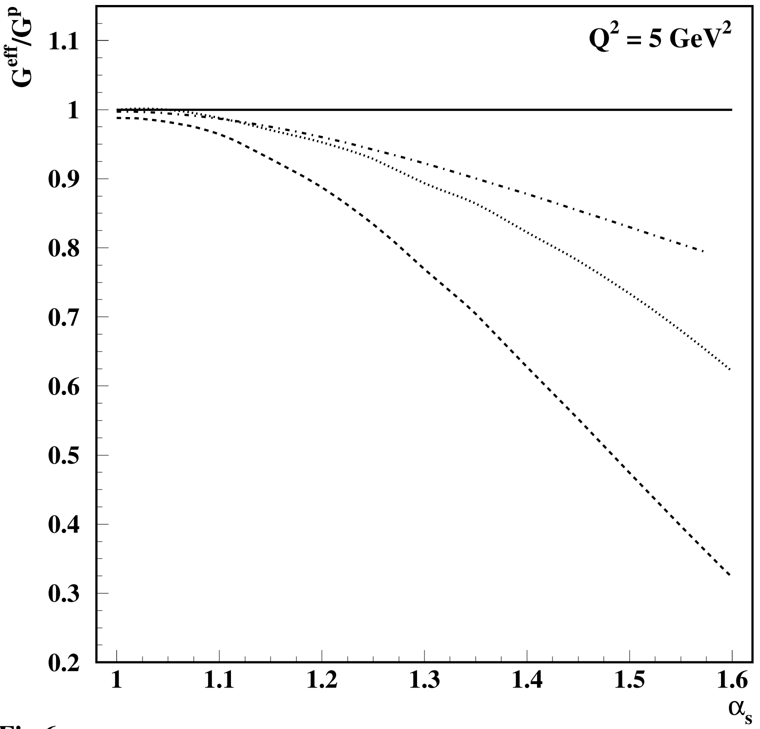

Fig.6

Figure 2: The α^s dependence of $G(\alpha_s, p_T, x_1, x_2, Q^2)$ with $x_1 = x/(2 - \alpha_s) = 0.6$ and $x_2 = x/(2 - \alpha_s) = 0.2$, for $p_T = 0$. $G^{eff}(\alpha^s, p_t, x_1, x_2, Q^2)$ is normalized to $G^{eff}(\alpha^s, p_t, x_1, x_2, Q^2)$ calculated with the free nucleon structure function. The dashed line is the PLC suppression model, dotted is the rescaling model and dot-dashed the Binding model

3 The Experiment

We are proposing to measure the semi-inclusive $D(e, e', N)X$ cross section ratio over a grid of x and α^s to access the structure function ratio $G(\alpha^s, p_t, x_1, x_2, Q^2)$ defined in equation 14. Each of the two semi-inclusive $D(e, e', N)X$ cross sections going into the ratio will be normalized to inclusive $D(e, e')$ cross sections as outlined below.

- We will use inclusive $D(e, e')$ data we gather simultaneously with $D(e, e', N)X$ coincidence data to normalize the $D(e, e', N)X$ cross section.
- The $D(e, e', N)X$ and $D(e, e')$ yields will be divided into x and Q^2 bins using identical cuts. Then the $D(e, e', N)X$ yield will be divided by the $D(e, e')$ yield bin by bin. This division will remove all normalization uncertainties on the electron detection side such as the luminosity, BigBite acceptance and efficiency.
- The normalized $D(e, e', N)X$ yield will then be subdivided into bins in α^s. At each α^s bin, the normalized yield from different bins in x will be divided by the normalized yield from the $x/(2 - \alpha^s) = 0.2$ bin. This normalization will divide out the deuteron spectral function, neutron detection efficiency and neutron

detector solid angle at each α^s bin. Thus this final ratio of $D(e,e',N)X$ yields will be equal to the cross section ratio

$$G = \frac{\sigma(D(e,e',N)X)_{(x_1/(2-\alpha^s),\alpha^s,p_t,Q_1^2)}}{\sigma(D(e,e',N)X)_{(x_2/(2-\alpha^s)=0.2,\alpha^s,p_t,Q_2^2)}} \tag{15}$$

within a systematic uncertainty only limited by the inclusive $D(e,e')$ structure function world data. In the kinematic region of the proposed experiment, these structure functions are known approximately to 1% level [55].

In the next few sections we address the remaining important issues related to the spectator nucleon approach:

3.1 Final State Interaction and p_t dependence issues

In the extreme backward neutron kinematics we are proposing for this experiment the FSI - the re-scattering of the spectator neutron by the remnants of the struck proton - have been shown to be suppressed [28, 29]. An estimate made by Melnitchouk *et al* for extreme backward kinematics indicate that for small p_t ($p_t \approx 0.1$ GeV) and $\alpha^s < 1.5$, the FSI contribution to $D(e,e',N)X$ is less than 5%. The proposed neutron detection system for this experiment covering the backward hemisphere is optimized for to detect neutrons with low p_t. Furthermore, we have used a kinematic cut at $p_t < 0.2$ GeV in our rate estimates and will use a similar cut in the data analysis to remove high p_t neutrons. Figure 3 shows the simulated p_t distributions for our six α^s bins. For low α^s bins we will further bin the data in several p_t bins to study the p_t dependence. If there is larger than expected dependence on p_t, this study will allow us to use more restrictive cuts to limit the data to even smaller values of p_t and to interpolate the measured values to $p_t = 0$

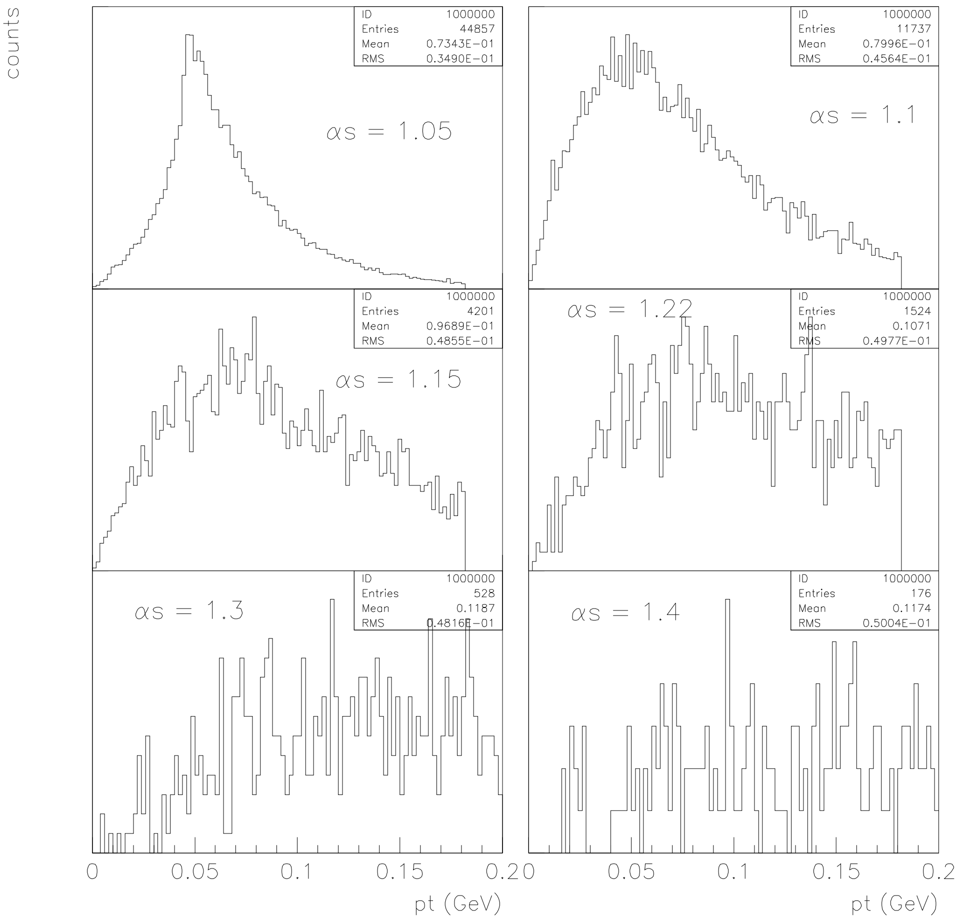

Figure 3: Simulated p_t distributions for our six α^s bins, with the kinematic cut at $p_t < 0.2$

3.2 Neutron creation due to Target Fragmentation and Sullivan Process

The fragmentation of low momentum neutrons from the proton debris is strongly suppressed in the extreme backward neutron kinematics [50, 54]. The contamination of spectator neutrons due target fragmentation is expected to be negligible for the kinematics of the proposed experiment. Another possible way to get a slow backward going neutron is through the Sullivan process, where the electron scatters off a π^+ in the pion cloud of the proton or off a π^0 in the pion cloud of the neutron. The cross section for this process was measured through leading neutron detection at HERA [56]. The cross section data for this process is incorporated in to *ep* collision Monte-Carlo Simulation program **RAPGAP** [57]. For the kinematics of the proposed experiment the contamination of spectator neutrons due to Sullivan process is expected to be less than 10 %.

We will measure the level of contamination due to target fragmentation and Sullivan process during our experiment by measuring the $H(e,e',N)X$ cross section with the neutron detection system in the identical configuration to the Deuterium runs. We will use the results from this run to calibrate **RAPGAP** simulation for our kinematics and then will use it to correct the measured $D(e,e',N)X$ cross sections bin by bin.

3.3 Experimental Setup

We will use a beam energy of 6 GeV. A low beam current and a thin - 1 cm long - liquid deuterium target would be used to achieve a luminosity of 4×10^{35} cm^{-2}s^{-1}. The experimental setup is shown in the schematic diagram of figure 4. The scattered electrons will be detected in the BigBite spectrometer at 35°. The backward going recoil neutrons will be detected using a combination of a especially designed low energy neutron detector and the GEN neutron detector [49].

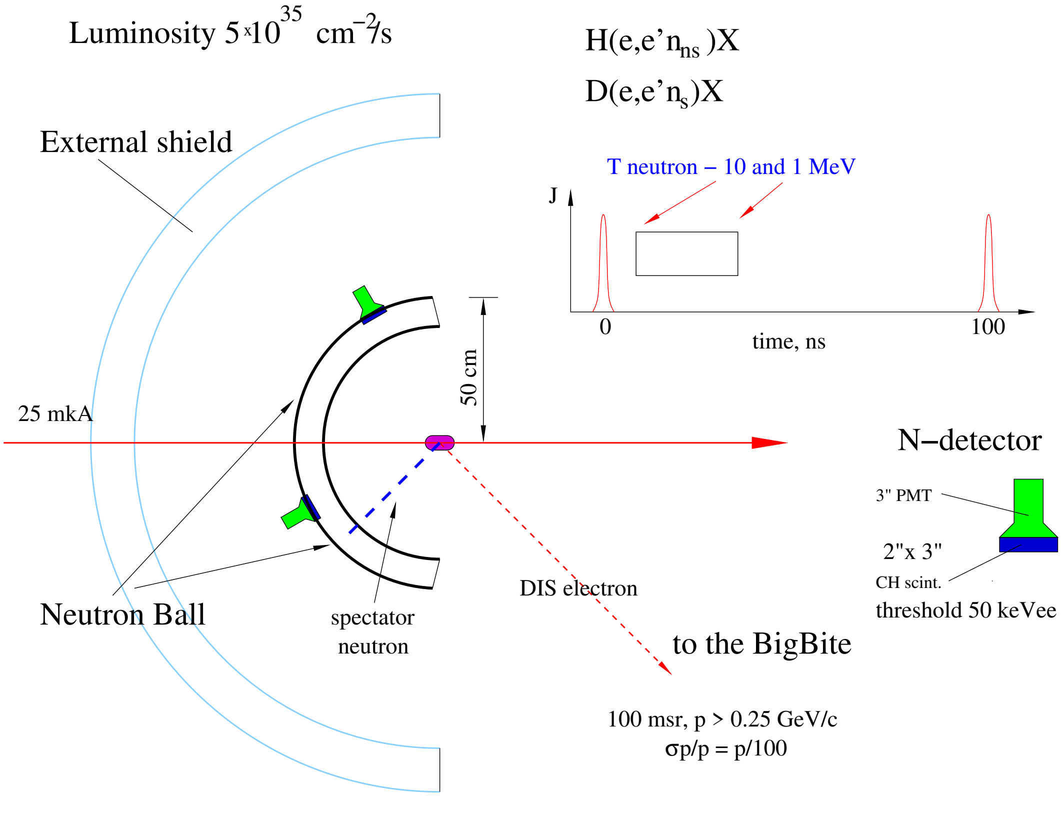

Figure 4: Schematic diagram of the proposed experimental setup

3.4 BigBite Spectrometer

The electrons will be detected in the BigBite spectrometer. Large angular and momentum acceptances of BigBite provide a combine gain factor of 30-50 in comparison with the Hall A High Resolution Spectrometers (HRS). This is the first key experimental factor that makes the proposed experiment possible. Large acceptance allows us to use the low luminosity required for very slow neutron detection. Furthermore, due to the wide momentum acceptance of BigBite all the data will come from a single field setting of the spectrometer. In the proposed momentum range, 0.5 GeV/c to about 2.2 GeV/c, the momentum resolution of the BigBite spectrometer would be between 0.5% and 2%. This is sufficient for the proposed measurement which relies on normalization to the free proton.

Due to relatively low luminosity, the expected rates at the BigBite detectors for this experiment is much lower than the rates for other BigBite experiments.

The only new addition to the BigBite spectrometer this experiments demands is a gas Čerenkov counter. The worst case pion to electron ratio we expect for this experiment is about 10:1. With the combination of a gas Čerenkov counter and the BigBite shower counter, which is already under construction, we plan to achieve a pion rejection ratio of about 1000. This is more than adequate to reject the pions for this experiment.

3.4.1 Shower detector

The shower detector for the BigBite spectrometer is under construction by the GEn collaboration. It consists of the preshower and shower sections made out of the lead-glass counters. A Total of 250 counters are used in that detector. A pion rejection factor of 30 is expected for this detector with an electron detection efficiency of 98%.

3.4.2 Gas Čerenkov counter

For the high luminosity of $1 \cdot 10^{37}$ expected in the GEn experiment the BigBite detector package includes three drift chambers. The role of the middle chamber is to ensure multi track reconstruction at high rates. At the luminosity of the proposed experiment we can remove the middle chamber. The space between remaining chambers of 60 cm allows us to insert a 50-60 cm gas Čerenkov counter with expected pion rejection factor of roughly 100. We plan to use a configuration similar to Hall A HRS gas Čerenkov counters with segmentation into 10 PMTs. Expected cost of this detector is less than $50k.

3.5 Recoil neutron detection

The second key experimental component of our proposal, which allows us to use sufficiently high luminosity, is a low duty factor regime of the electron beam. The G0 experiment successfully used a beam structure with pulses 32 ns apart. An even larger time structure of 48 ns[1] will be used in our experiment.

For the detection of neutrons with kinetic energies between 1 MeV and 15 MeV ($50 < p^s < 170$ MeV/c) we are proposing to construct a special low energy neutron

[1] This corresponds to a pulse rate of 20 MHz. If the accelerator technical issues force us to use a 16 MHz structure, it will change the projections presented here only by a small amount

detector - neutron hemisphere- based on liquid scintillators. This detector would be placed at 50 cm from the target to cover most of the backward hemisphere. The total solid angle would be approximately 4 sr.

A Monte-Carlo calculation performed for the proposed neutron detector[52] indicates that we can block all low energy protons and most photons coming from the target by using just a 5 mm thick lead shield. These simulations also show that with a 50 keVee threshold on neutron detectors we can detect neutrons down to about 1 MeV kinetic energy.

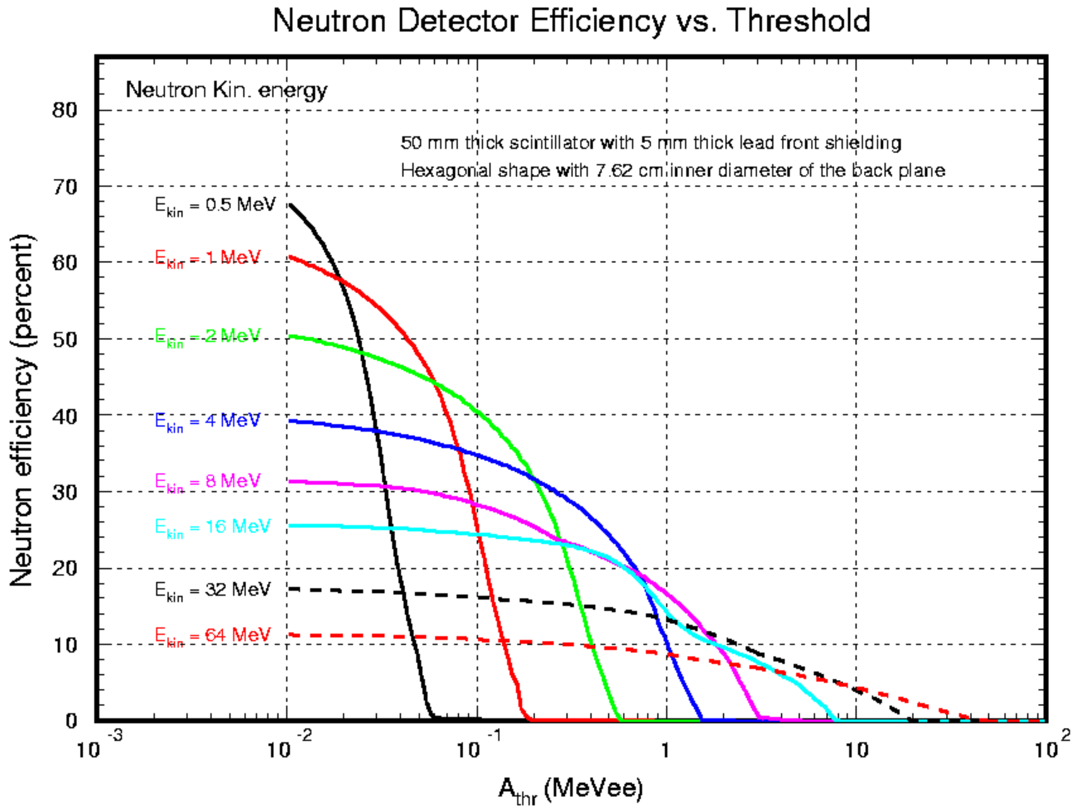

Figure 5: Preliminary MC results for neutron efficiency.

At a luminosity of 5×10^{35} the amount of background was found from MC simulations preformed by Pavel Degtiarenko [53] (see figure ??). A few nano seconds after the beam bunch passes through the target the photons and most of other particles will pass through the neutron detectors. We found that given a segmentation of the neutron detector into 175 counters, less than 10% of them will get a hit from these particles. These counters will become dead for about 30-50 ns after the hit. This dead time of about 10% will be accurately measured. Neutrons with kinetic energies between 1 MeV and 15 MeV will arrive at the detector between 12 ns and 45 ns. In that time interval the main background will be low energy neutrons.

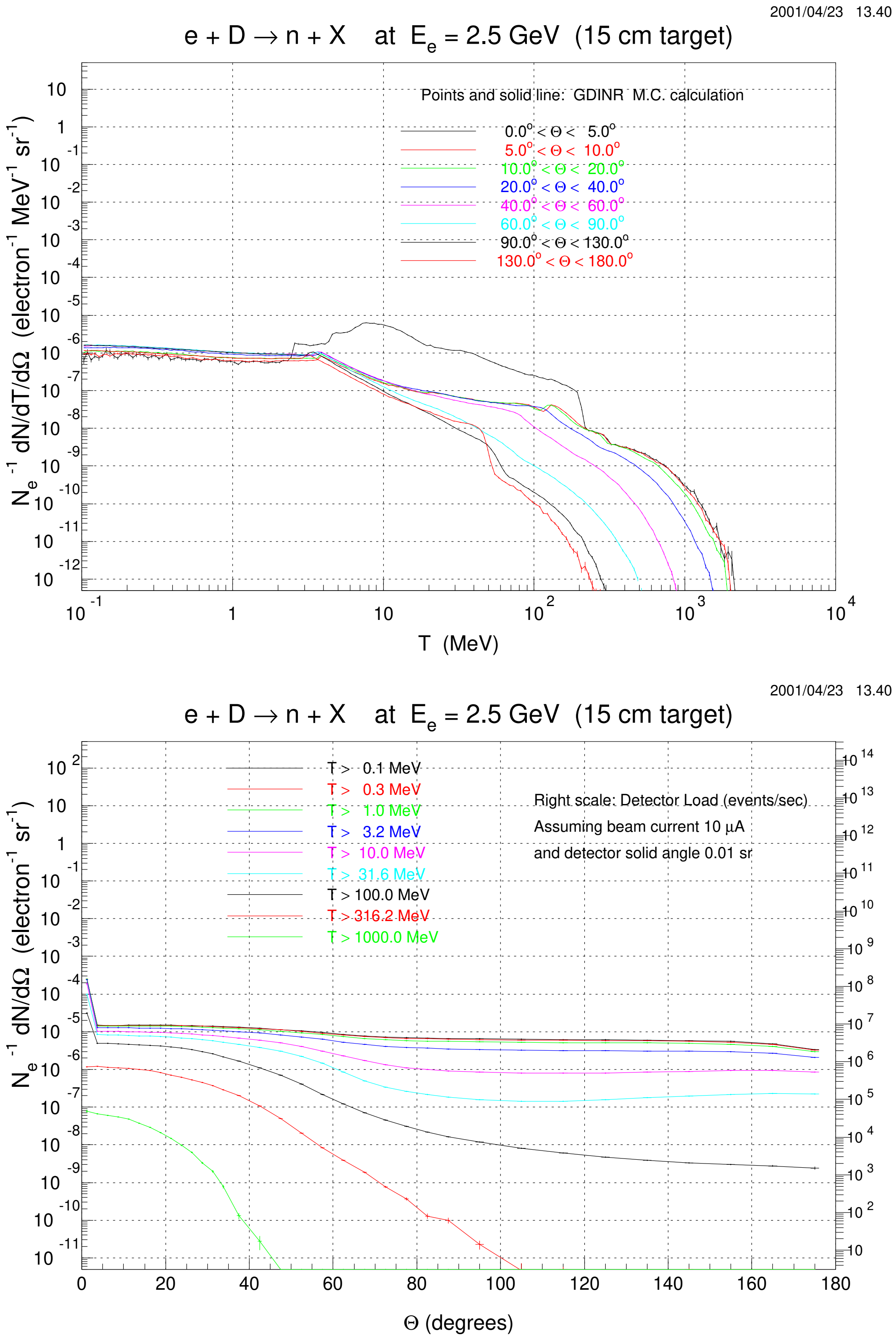

Figure 6: Monte-Carlo results for background neutron rates for a deuteron target.

Figure 6 shows the Monte-carlo simulation of expected background neutron rates. Interactions of the target with primary electrons as well as with real and quasi-real photons accompanying the beam have been considered in this Monte-Carlo. The signal to noise ratio analysis for different neutron momentum ranges is presented in table 1. The second column of the table shows simulated background rate (evaluated for the proposed luminosity of 5×10^{35} and the neutron detector solid angle of 4 sr), for several ranges of neutron kinetic energies considered in this proposal. Let the background neutron rate for a momentum range Δp be $B_{\Delta p}$. Then the probability of getting a background neutron in momentum range Δp followed by a beam bunch that produced a detected electron is given by $B_{\Delta p}/(20 \times 10^6)$ (for the proposed 20 MHz beam structure). This per pulse background hit probability is given in the third column of the table. The probability of getting a real coincidence for a neutron in the momentum range Δp is equal to the integrated strength of the (normalized) neutron momentum distribution over Δp, times the fraction of the full solid angle covered by the neutron detector [2]. This signal probability is given in the forth column of the table followed by the signal to noise ratio in the fifth column.

Kinetic energy range MeV/c	Background n rate s^{-1}	Background probability	Signal probability	signal to noise ratio
1 - 3.2	3.4×10^6	1.7×10^{-1}	1.1×10^{-1}	1:1.6
3.2 - 10	2.6×10^5	1.3×10^{-1}	8.7×10^{-2}	1:1.5
10- 20	9×10^5	4.5×10^{-2}	2.9×10^{-2}	1:1.6
20- 50	5×10^5	2.4×10^{-2}	1.7×10^{-2}	1:1.5
50- 79	1×10^5	4.5×10^{-3}	3.3×10^{-3}	1:1.4

Table 1: Signal to noise ratio analysis for different neutron momentum ranges

As the table indicates the signal to noise ratio over the entire momentum range of the neutron is about 1:1.5. We will use the multi-hit feature of the TDCs to measure the background with high accuracy. A multi-hit TDC with a gate width of about 1 μs will register random coincidence spectra for 20 beam bunches following a bunch that generates an electron hit. This will allow us to determine background level at every neutron momentum with a statistical error about 5 times smaller than the statistical error we project for the signal. Thus at the projected signal to noise ratio of 1:1.5, our statistical error will increase only by a factor of $\sqrt{2.5}$ due to background subtraction. This uncertainty of factored into all projected statistical errors given in this proposal.

For the detection of neutrons with kinetic energies between than 15 MeV and 65 MeV we will use the GEn neutron detector installed behind the neutron-hemisphere. This detector be at an average distance of 3 meters from the target and will cover a solid angle of about 3 sr.

[2] Note that the neutron detection efficiency enters both probabilities and drops out of the signal to noise ratio.

3.5.1 Low energy neutron detector hardware

A neutron detector very similar to the one proposed for this experiment was recently constructed[51] by Blaine Norum and Brad Sawatzki, members of this collaboration from the University of Virginia group. This low energy neutron detector, nick named **BLOWFISH** was successfully used to detect neutrons with kinetic energies as low as 0.65 MeV in a low energy D(γ,n) experiment at **HIGS**. The Blowfish detector (Fig 7) consists of 88 BC-505 liquid scintillator cells mounted on the surface of a 20 cm radius imaginary sphere. Each cell (Fig 8) consists of a scintillation box $8.2 \times 8.2 \times 7.1$ cm^2 constructed of Lucite. The scintillation box is then coupled through a light guide to the PMT and the Base.

Liquid scintillators are known for their obnoxious chemical properties and hazardously low flash points. However, liquid scintillator BC-505 was found to be much easier to work with than the more traditional liquid scintillator NE-213. Furthermore BC-505 has a higher flash point than NE-213 and allows safer working conditions.

The BLOWFISH detector was successfully commissioned and operated in 2002. The experimentally measured neutron detections efficiencies for Blowfish cells agree well with the simulations and are around between 40% for neutrons with kinetic energies above 1 MeV.

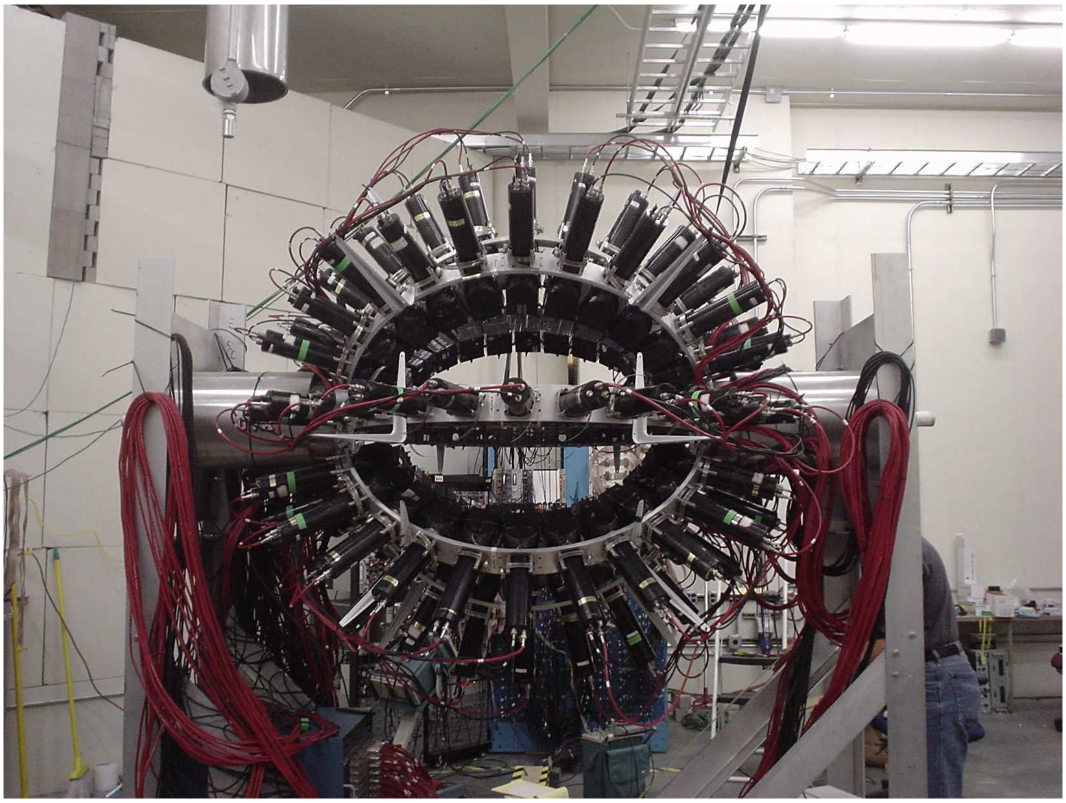

Figure 7: BLOWFISH low energy neutron detector at HIGS

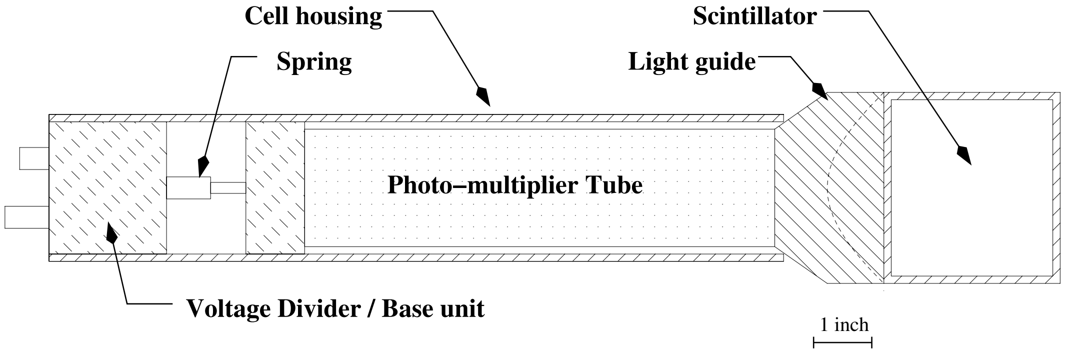

Figure 8: A single neutron cell from BLOWFISH

The expertise of Blaine Norum and Brad Sawatzki in the design, construction and successful operation of the ultra-low energy neutron detectors would be invaluable in the construction of neutron detectors for the proposed experiment. We will base the design of neutron detection cells on the Blowfish cells design. The active area of the proposed neutron hemisphere is approximately 1 m^2, and it will consists of roughly 175 Blowfish-type cells. Table 2 shows the estimated cost of 175 assembled cells, based on the very recent experience of the University of Virginia group. Allowing a 35% increase to meet inflation and contingency and adding \$ 30,000 to cover the cost of 175 TDC and ADC channels, the total cost of the proposed neutron detector is expected to be around \$ 150,000.

Quantity	Description	Unit Cost	Sub total
15 gal	BC-505 liquid scintillator	\$300	\$4,500
175	PMT	\$250	\$43,750
175	Base+housing units	\$175	\$30,625
175	Lucite box + light guide	\$50	\$8,750
175	fiber optics for gain monitor	\$15	\$2,625
			\$90,250

Table 2: Breakdown of estimated costs for the proposed neutron detector

3.5.2 Low energy neutron detector tests

The **HIGS** facility shutdown scheduled for 2005 allows us to borrow several Blowfish neutron detector cells to test in beam in Hall A. We have already made a request to Hall A leader for 12 hours of beam time during facility development time in April 2005. This is during the Short-Range correlation experiment in Hall A when the BigBite spectrometer will be operational. We will use this beam time to test 4 Blowfish neutron cells for singles rates and also for coincidence rates with the BigBite electron trigger.

Furthermore, with the PAC endorsement of this proposal, this collaboration will be able to seek funding for a prototype neutron detector that covers 1/4 solid angle of the full proposed detector in the next few months. We are planing to design, construct and test this prototype detector in the Summer 2005.

3.6 Kinematics and rate estimates

All kinematic settings for this experiment are with $E_0 = 6$ GeV and $\theta_e = 35°$. We have assumed a solid angle of 96 msr for the BigBite spectrometer at 35°. A kinematic cut $p_t < 0.2$ GeV/c was used to ensure that the transverse momentum was small. To select DIS events $Q^2 > 1$ GeV^2 and $W'2 > 4$ GeV^2 cuts will be used. An average neutron efficiency of 30% was assumed.

Table 3 shows the beam time allocation for different settings. Tables 4 and 5 give the Q^2, $W^{2\prime}$ and statistics for each x', α_s for the low and high spectator momentum settings respectively.

setting	Target	Nuetron momentum	Neutron Detector	Time (Hours)
low p^n $D(e, e'n)$	LD2	0.05-0.17 GeV/c	Neutron hemisphere	75
higher p^n $D(e, e'n)$	LD2	0.15-0.4 GeV/c	Gen detector	300
low p^n $H(e, e'n)$	LH2	0.05-0.17 GeV/c	Neutron hemisphere	5
higher p^n $H(e, e'n)$	LH2	0.15-0.4 GeV/c	Gen detector	30
System checkout				20

Table 3: Beam time breakdown for production and background running as well as experimental setup checks

α_s	E′ (GeV)	Q^2 (GeV/c)^2	x'	$W^{2\prime}$ (GeV/c^2)^2	Rate (events per hour)	Total counts	Stat. uncertainty
1.04	0.45	0.98	0.10	10.0	3206.9	240515	0.003
1.04	0.60	1.30	0.13	9.4	2661.7	199627	0.004
1.04	0.75	1.63	0.17	8.8	2286.7	171499	0.004
1.04	0.90	1.95	0.21	8.2	1999.7	149979	0.004
1.04	1.05	2.28	0.25	7.6	1756.0	131701	0.004
1.04	1.20	2.60	0.30	7.0	1529.0	114677	0.005
1.04	1.35	2.93	0.35	6.4	1307.5	98060	0.005
1.04	1.50	3.26	0.40	5.8	1089.1	81683	0.006
1.04	1.65	3.58	0.45	5.2	877.3	65795	0.006
1.04	1.80	3.91	0.51	4.6	678.5	50890	0.007
1.04	1.95	4.23	0.58	4.0	500.1	37506	0.008
1.04	2.10	4.56	0.65	3.4	346.1	25956	0.010
1.10	0.50	1.09	0.11	9.3	853.3	63994	0.006
1.10	0.65	1.41	0.15	8.7	717.2	53787	0.007
1.10	0.80	1.74	0.19	8.1	618.8	46412	0.007
1.10	0.95	2.06	0.24	7.5	539.7	40480	0.008
1.10	1.10	2.39	0.28	6.9	468.9	35166	0.009
1.10	1.25	2.71	0.33	6.3	400.9	30068	0.009
1.10	1.40	3.04	0.39	5.7	334.3	25071	0.010
1.10	1.55	3.36	0.44	5.1	269.7	20227	0.011
1.10	1.70	3.69	0.50	4.5	209.0	15677	0.013
1.10	1.85	4.01	0.57	4.0	154.5	11587	0.015
1.10	2.00	4.34	0.64	3.4	107.4	8057	0.018
1.15	0.55	1.19	0.13	8.6	1015.0	76123	0.006
1.15	0.70	1.52	0.18	8.0	860.5	64537	0.006
1.15	0.85	1.84	0.22	7.5	743.4	55756	0.007
1.15	1.00	2.17	0.27	6.9	643.9	48295	0.007
1.15	1.15	2.50	0.32	6.3	551.1	41332	0.008
1.15	1.30	2.82	0.37	5.7	460.9	34567	0.009
1.15	1.45	3.15	0.42	5.1	373.4	28006	0.010
1.15	1.60	3.47	0.49	4.6	290.9	21818	0.011
1.15	1.75	3.80	0.55	4.0	216.4	16227	0.013
1.15	1.90	4.12	0.62	3.4	151.9	11390	0.015

Table 4: Q^2, $W^{2\prime}$ and statistics for each x', α_s bin in the low p^n $D(e,e'n)$ running (75 hours). The statistics given have been calculated using the neutron detector solid angle (4 sr), neutron detection efficiency (30%), and the deuteron spectral strength integrated over the α_s bin width. A $p_t < 0.2$ GeV/c was has been applies. The statistical errors shown included an extra factor of $\sqrt{2.5}$ to account for background subtraction uncertainty.

α_s	E′ (GeV)	Q^2 (GeV/c)^2	x'	$W^{2\prime}$ (GeV/c^2)^2	Rate (events per hour)	Total counts	Stat. uncertainty
1.22	0.45	0.98	0.11	8.5	98.3	29486	0.009
1.22	0.60	1.30	0.16	7.9	81.3	24375	0.010
1.22	0.75	1.63	0.20	7.3	69.2	20752	0.011
1.22	0.90	1.95	0.25	6.8	59.5	17847	0.012
1.22	1.05	2.28	0.30	6.2	50.8	15238	0.013
1.22	1.20	2.60	0.35	5.6	42.5	12740	0.014
1.22	1.35	2.93	0.41	5.1	34.4	10326	0.016
1.22	1.50	3.26	0.47	4.5	26.8	8049	0.018
1.22	1.65	3.58	0.54	3.9	20.0	5991	0.021
1.22	1.80	3.91	0.61	3.4	14.0	4212	0.025
1.30	0.47	1.02	0.13	7.9	31.3	9379	0.017
1.30	0.62	1.35	0.17	7.3	25.9	7773	0.018
1.30	0.77	1.67	0.22	6.8	22.0	6596	0.020
1.30	0.92	2.00	0.27	6.2	18.7	5615	0.021
1.30	1.07	2.32	0.33	5.6	15.7	4709	0.023
1.30	1.22	2.65	0.39	5.1	12.8	3839	0.026
1.30	1.37	2.97	0.45	4.5	10.1	3015	0.029
1.30	1.52	3.30	0.52	4.0	7.5	2264	0.034
1.30	1.67	3.62	0.59	3.4	5.4	1610	0.040
1.40	0.40	0.87	0.11	7.6	18.4	5515	0.022
1.40	0.60	1.30	0.18	6.9	14.0	4202	0.025
1.40	0.80	1.74	0.25	6.2	11.1	3343	0.028
1.40	1.00	2.17	0.32	5.4	8.8	2630	0.031
1.40	1.20	2.60	0.40	4.7	6.6	1969	0.036
1.40	1.40	3.04	0.49	4.0	4.6	1369	0.043
1.40	1.60	3.47	0.59	3.3	2.9	867	0.054

Table 5: Same as in table for higher p^n $D(e, e'n)$ setting (300 hours)

Figure 9 shows the projected uncertainties for the $x = 0.6$ bin as a function of α^s for the 35° setting. Figures 10,11 show the x dependence for four bins of α^s.

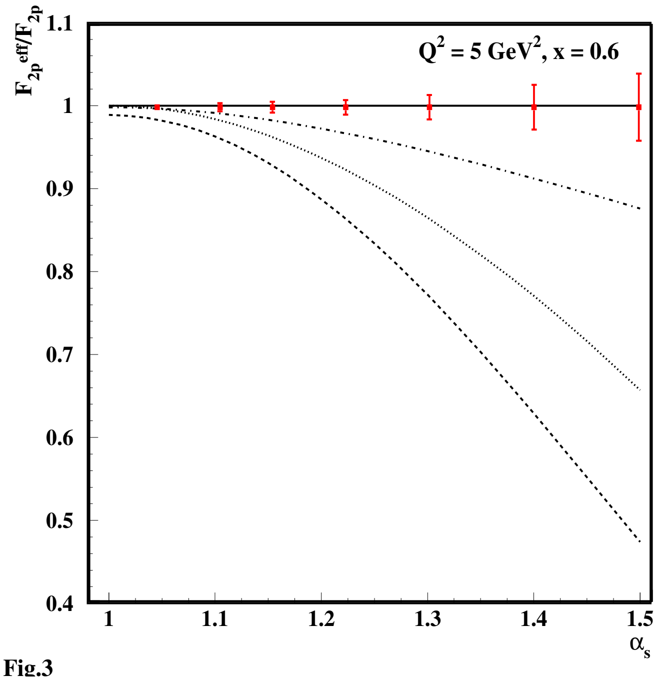

Figure 9: Projected uncertainties. Theory curves from Melnitchouk *et al.*, evaluated at $Q^2 = 5$ GeV/c^2 : Dashed: PLC suppression model; Dotted: Rescaling model, Dot-dashed: nuclear binding model

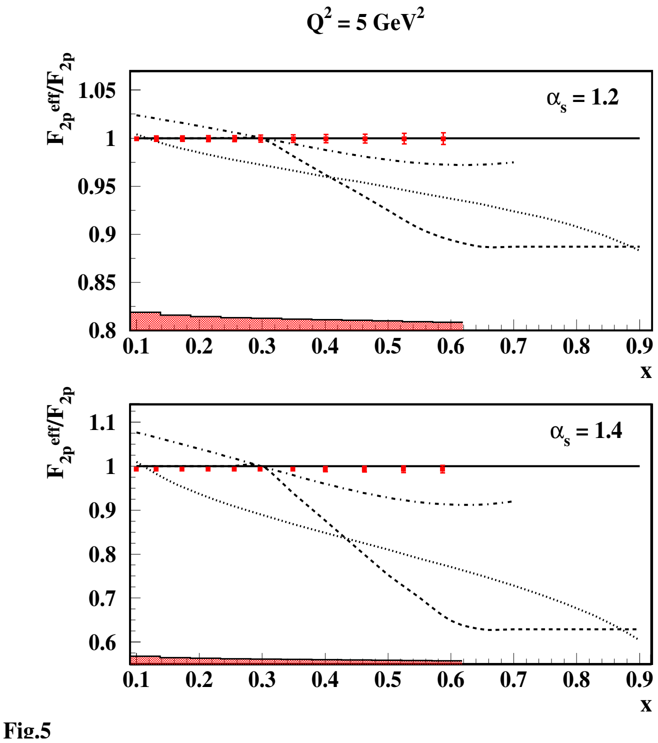

Figure 10: Projected uncertainties at different bins of α^s

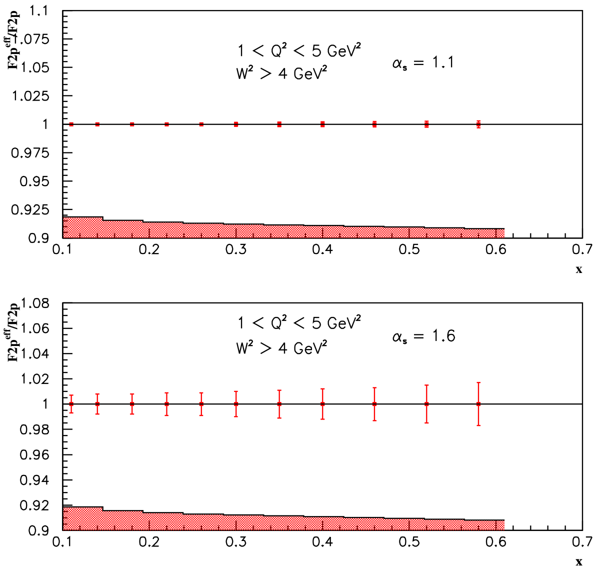

Figure 11: Projected uncertainties at different bins of α^s

Including 45 hours for calibrations and spectrometer movement we would like to request 300 hours for the proposed measurement. In addition to this we would like to request 50 hours of beam time before the experiment to commission the neutron detector.

4 Summary and Request

We are proposing a measurement of the cross section ratio

$$\frac{\sigma(D(e,e',N)X)_(x,\alpha^s,p_t,Q^2)}{\sigma(p(e,e')X)_(x',Q^2)}. \tag{16}$$

to study the variation of the ratio of bound proton cross section to the free proton cross section as a function of the spectator neutron momentum at five values of x up to $x = 0.6$. The variation of this ratio will help distinguish between different theoretical explanations of the EMC effect and may provide crucial clues to solve a mystery that has puzzled both nuclear physics and particle physics communities for over twenty years. We are treating the proposed measurement at a pilot measurement. Given the success of the proposed experiment, it has the potential to open up an important experimental initiative at 12 GeV to probe the EMC effect up to $x < 0.8$.

We are requesting 350 hours to perform this breakthrough measurement.

References

[1] J. J. Aubert *et al.* (EM Collaboration), Phys. Lett. B **123**, 275 (1983).

[2] S. Dasu *et al.*, Phys. Rev. D **49**, 5641 (1994).

[3] J. Gomez *et al.*, Phys. Rev. D **49**, 4348 (1994).

[4] A. C. Benvenuti *et al.* (BCDMS Collaboration), Phys. Lett. B **189**, 483 (1987).

[5] J. Ashman *et al.* (EM Collaboration), Phys. Lett. B **202**, 603 (1988); Z. Phys. C **57**, 211 (1993).

[6] D. F. Geesaman, K. Saito and A. W. Thomas, Ann. Rev. Nucl. Part. Sci. **45**, 337 (1995).

[7] J. Arrington (Spokesperson), Jefferson Lab Experiment 03-103.

[8] W. Melnitchouk, M. Sargsian and M. I. Strikman, Z. Phys. A **359**, 99 (1997)

[9] S. E. Kuhn and K. A. Griffioen (Spokespersons), Jefferson Lab Experiment 94-102.

[10] W. Melnitchouk and A. W. Thomas, Phys. Lett. B **377**, 11 (1996)

[11] H. Fenker, C. Keppel, S. E. Kuhn and W. Melnitchouk (Spokespersons), Jefferson Lab Experiment 03-012

[12] Proceedings of Workshop "Future Physics at HERA", Sep. 95 – May 96, DESY, Hamburg (1996); G. van der Steenhoven, private communication.

[13] L. L Frankfurt and M. I. Strikman, Phys. Rep. **76**, 217 (1981).

[14] W. Melnitchouk, A. W. Schreiber, and A. W. Thomas, Phys. Rev. D **49**, 1183 (1994).

[15] S. A. Kulagin, G. Piller, and W. Weise, Phys. Rev. C **50**, 1154 (1994).

[16] W. Melnitchouk, A. W. Schreiber, and A. W. Thomas, Phys. Lett. B **335**, 11 (1994).

[17] S. A. Kulagin, W. Melnitchouk, G. Piller, and W. Weise, Phys. Rev. C **52**, 932 (1995).

[18] W. W. Buck and F. Gross, Phys. Rev. D **20**, 2361 (1979); J. W. Van Orden, N. Devine, and F. Gross, Phys. Rev. Lett. **75**, 4369 (1995); E. Hummel and J. A. Tjon Phys. Rev. C **49**, 21 (1994).

[19] W. Melnitchouk, G. Piller, and A. W. Thomas, Phys. Lett. B **346**, 165 (1995); G. Piller, W. Melnitchouk, and A. W. Thomas, Phys. Rev. C **54**, 894 (1996).

[20] L. L. Frankfurt and M. I. Strikman, Phys. Lett. **64** B, 435 (1976).

[21] P. V. Landshoff and J. C.Polkinghorne, Phys. Rev. D **18**, 158 (1978).

[22] L. L. Frankfurt and M. I. Strikman, Phys. Rep. **160**, 235 (1988).

[23] G. P. Lepage and S. J. Brodsky, Phys. Rev. D **22**, 2157 (1980).

[24] M. Lacombe *et al.*, Phys. Rev. C **21**, 861 (1990).

[25] R. Machleidt, K. Holinde, and Ch. Elster, Phys. Rep. **149**, 1 (1987).

[26] M. I. Strikman, M. Tverskoy, and M. Zhalov, in Proceedings of Workshop "Future Physics at HERA", Hamburg, pp.1085-1088 (1996), nucl-th/9609055.

[27] E665 Collaboration, M. R. Adams *et al.*, Phys. Rev. Lett. **74**, 5198 (1995).

[28] L. L. Frankfurt, G. A. Miller, W. R. Greenberg, M. M. Sargsyan, and M. I. Strikman, Z. Phys. A **352**, 97 (1995).

[29] L. L. Frankfurt, G. A. Miller, W. R. Greenberg, M. M. Sargsyan, and M. I. Strikman, Phys. Lett. B **369**, 201 (1996).

[30] L. L. Frankfurt and M. I. Strikman, Nucl. Phys. **B250**, 1585 (1985).

[31] C. E. Carlson and K.E. Lassilla and P.U. Sukhatme, Phys. Lett. B **263**, 277 (1992).

[32] C. Ciofi degli Atti and S. Simula, Few Body Systems **18**, 55 (1995).

[33] S. V. Akulinichev, S. A. Kulagin and G. M. Vagradov, Phys. Lett. **158** B, 485 (1985); S. A. Kulagin, Nucl. Phys. **A500**, 653 (1989).

[34] G. V. Dunne and A. W. Thomas, Nucl. Phys. **A446**, 437c (1985).

[35] M. Ericson and A. W. Thomas, Phys. Lett. B **128**, 112 (1983).

[36] B. L. Friman, V. R. Pandharipande, and R. B. Wiringa, Phys. Rev. Lett. **51**, 763 (1983); E. L. Berger, F. Coester, and R. B. Wiringa, Phys. Rev. D **29**, 398 (1984).

[37] H. Jung and G. A. Miller, Phys. Lett. B **200**, 351 (1988).

[38] C. Ciofi degli Atti and S. Liuti, Phys. Lett. B **225**, 215 (1989).

[39] L. P. Kaptari *et al.*, Nucl. Phys. **A512**, 684 (1990); W. Melnitchouk and A. W. Thomas, Phys. Rev. D **47**, 3783 (1993).

[40] R. P. Bickerstaff and A. W. Thomas, J. Phys. G **15**, 1523 (1989).

[41] S. Huang and J. Tjon, Phys. Rev. C **49**, 1702 (1994); N. Ishii, W. Bentz, and K. Yazaki, Phys. Lett. B **301**, 165 (1993); H. Meyer, Phys. Lett. B **337**, 37 (1994); C. M. Shakin and W.-D. Sun, Phys. Rev. C **50**, 2553 (1994).

[42] M. R. Frank, B. K. Jennings and G. A. Miller, Phys. Rev. C **54**, 920 (1996).

[43] L. L. Frankfurt M. M. Sargsian and M. I. Strikman, Z. Phys. A **335**, 431 (1990).

[44] F. E. Close, R. G. Roberts and G. G. Ross, Phys. Lett. B **129**, 346 (1983).

[45] O. Nachtmann and H. J. Pirner, Z. Phys. C **21**, 277 (1984).

[46] R. L. Jaffe, F. E. Close, R. G. Roberts and G. G. Ross, Phys. Lett. B **134**, 449 (1984).

[47] F. E. Close *et al.*, Phys. Rev. D **31**, 1004 (1985).

[48] G. Güttner and H. J. Pirner, Nucl. Phys. **A457**, 555 (1986).

[49] G. Cates, K. McCormick, B. Reitz, and B. Wojtsekhowski, Jefferson Lab experiment E02-013.

[50] C. Ciofi degli Atti and S. Simula, Phys. Lett. B **319** (1993) 23.

[51] B. Swatski, Ph. D Thesis, University of Virginia (2004).

[52] P. Degtiarenko, Private Communications.

[53] P. Degtiarenko, Private Communications.

[54] S. Simula, Phys. Lett. B **387**, 245 (1996)

[55] L. W. Whitlow, Ph. D Thesis, Stanford University (1990) (SLAC-0357); L. W. Whitlow, E. M. Riordan, S. Dasu, S. Rock and A. Bodek, Phys. Lett. B **282**, 475 (1992).

[56] G. Levman, Nucl. Phys. B **642**, 3 (2002). [arXiv:hep-ph/0208059].; K. Borras [H1 and ZEUS Collaborations], Acta Phys. Polon. B **33** (2002) 3219.

[57] H. Jung, Comput. Phys. Commun. **86**, 147 (1995).